

DESIGN OF FINITE FIELD MULTIPLIERS WITH CRC-BASED ERROR DETECTION CONSTRUCTIONS IN CRYPTOGRAPHY APPLICATIONS

¹ YALAGANDHULA EESWARASAI, ² Mr. G. BABU

¹ PG Scholar, Dept. of ECE, Vaagdevi College of Engineering, Warangal, Telangana, India.

² Assistant professor, Dept. of ECE, Vaagdevi College of Engineering, Warangal, Telangana, India.

¹ eeswarasai@gmail.com, ² babugundlapally@gmail.com

Abstract— In this paper Finite-field multiplication has received prominent attention in the literature with applications in cryptography and error-detecting codes. For many cryptographic algorithms, this arithmetic operation is a complex, costly, and time-consuming task that may require millions of gates. In this work, we propose efficient hardware architectures based on cyclic redundancy check (CRC) as error-detection schemes for post quantum cryptography (PQC) with case studies for the Luov cryptographic algorithm. Luov was submitted for the National Institute of Standards and Technology (NIST) PQC standardization competition and was advanced to the second round. The CRC polynomials selected are in-line with the required error-detection capabilities and with the field sizes as well. We have developed verification codes through which software implementations of the proposed schemes are performed to verify the derivations of the formulations. Additionally, hardware implementations of the original multipliers with the proposed error-detection schemes are performed over a Xilinx field-programmable gate array (FPGA), verifying that the proposed schemes achieve high error coverage with acceptable overhead.

Keywords— Cyclic redundancy check (CRC), fault detection, field-programmable gate array (FPGA), finite-field multiplication.

I. INTRODUCTION

Many modern, sensitive applications and systems use finite-field operations in their schemes, among which finite-field multiplication has received prominent attention. Finite-field multipliers perform multiplication modulo, an irreducible polynomial used to define the finite field. For post quantum cryptography (PQC), the inputs can be very large, and the finite-field multipliers may require millions of logic gates. Therefore, it is a complex task to implement such architectures resilient to natural and malicious faults; consequently, research has focused on ways to

eliminate errors and obtain more reliability with acceptable overhead [1]–[6]. Moreover, there has been previous work on countering fault attacks and providing reliability for PQC. Sarker et al. [7] used error-detection schemes of number theoretic transform (NTT) to detect both permanent and transient faults. Mozaffari-Kermani et al. [8] performed fault detection for stateless hash-based PQC signatures. Additionally, error-detection hash trees for stateless hash-based signatures are proposed in [9] to make such schemes more reliable against natural faults and help protecting them against malicious faults. In [10], algorithm-oblivious constructions are proposed through recomputing with swapped cipher text and additional authenticated blocks, which can be applied to the Galois counter mode (GCM) architectures using different finite-field multipliers in $G F(2^{128})$. Several countermeasures based on error-detection checksum codes and spatial/temporal redundancies for the NTRU encryption algorithm have been presented in [11].

Our proposed error-detection architectures are adapted to the Luov cryptographic algorithm [12]; however, they can be applied to different PQC algorithms that use finite-field multipliers. The Luov algorithm was submitted for National Institute of Standards and Technology (NIST) standardization competition [13] and was advanced to the second round [14]. Cyclic redundancy check (CRC) error-detection schemes are applied in our proposed hardware constructions to make sure that they are overhead-aware with high error coverage. Our contributions in this brief are summarized as follows.

1) Error-detection schemes for the finite-field multipliers $G F(2^m)$ with $m > 1$ used in the Luov cryptographic algorithm are proposed. These error-detection architectures are based on CRC-5. Additionally, we explore and study both primitive and standardized generator

polynomials for CRC-5, comparing their complexity.

2) We derive new formulations for the error-detection schemes of Luov's algorithm, performing software implementations for the sake of verifications. We note that such derivation covers a wide range of applications and security levels. Nevertheless, the presented schemes are not confined to these case studies.

3) The proposed error-detection architectures are embedded into the original finite-field multipliers. We perform the implementations using Xilinx field-programmable gate array (FPGA) family Kintex Ultrascale+ for device xcku5p-ffvd900-1-i to confirm that the schemes are overhead-aware and that they provide high error coverage.

II. RELATED WORK

a) Reliable hardware architectures for the third-round sha-3 finalist grostl benchmarked on fpga platform:

The third round of competition for the SHA-3 candidates is ongoing to select the winning function in 2012. Although much attention has been devoted to the performance and security of these candidates, the approaches for increasing their reliability have not been presented to date. In this paper, for the first time, we propose a high-performance scheme for fault detection of the SHA-3 round-three candidate Grostl which is inspired by the Advanced Encryption Standard (AES). We propose a low-overhead fault detection scheme by presenting closed formulations for the predicted signatures of different transformations of this SHA-3 third-round finalist. These signatures are derived to achieve low overhead and include one or multi-bit parities and byte/word-wide predicted signatures. The proposed reliable hardware architectures for Grostl are implemented on Xilinx Virtex-6 FPGA family to benchmark their hardware and timing characteristics. The results of our evaluations show high error coverage and acceptable overhead for the proposed scheme.

b) Reliable hardware architectures for cryptographic block ciphers led and height:

Cryptographic architectures provide different security properties to sensitive usage models. However, unless reliability of architectures is

guaranteed, such security properties can be undermined through natural or malicious faults. In this paper, two underlying block ciphers which can be used in authenticated encryption algorithms are considered, i.e., light encryption device and high security and lightweight block ciphers. The former is of the Advanced Encryption Standard type and has been considered area-efficient, while the latter constitutes a Feistel network structure and is suitable for low-complexity and low-power embedded security applications. In this paper, we propose efficient error detection architectures including variants of recomputing with encoded operands and signature-based schemes to detect both transient and permanent faults. Authenticated encryption is applied in cryptography to provide confidentiality, integrity, and authenticity simultaneously to the message sent in a communication channel. In this paper, we show that the proposed schemes are applicable to the case study of simple lightweight CFB for providing authenticated encryption with associated data. The error simulations are performed using Xilinx Integrated Synthesis Environment tool and the results are benchmarked for the Xilinx FPGA family Virtex-7 to assess the reliability capability and efficiency of the proposed architectures.

III. CYCLIC REDUNDANCY CHECK

The cyclic redundancy check, or CRC, is a technique for detecting errors in digital data, but not for making corrections when errors are detected. It is used primarily in data transmission. In the CRC method, a certain number of check bits, often called a checksum, are appended to the message being transmitted. The receiver can determine whether or not the check bits agree with the data, to ascertain with a certain degree of probability whether or not an error occurred in transmission. If an error occurred, the receiver sends a "negative acknowledgement" (NAK) back to the sender, requesting that the message be retransmitted.

The technique is also sometimes applied to data storage devices, such as a disk drive. In this situation each block on the disk would have check bits, and the hardware might automatically initiate a reread of the block when an error is detected, or it might report the error to software.

The material that follows speaks in terms of a "sender" and a "receiver" of a "message," but it should be understood that it applies to storage writing and reading as well.

IV. PROPOSED SYSTEM

The proposed system are five popular PQC algorithm classes: code-based, hash-based, isogeny-based, lattice-based, and multivariate-quadratic equation-based cryptosystems [15]. Code-based cryptography differs from others in that its security relies on the hardness of decoding in a linear error-correcting code. Hash-based cryptography creates signature algorithms based on the security of a selected cryptographic hash function. The security of isogeny-based cryptography is based on the hard problem to find an isogeny between two given super singular elliptic curves. Lattice-based cryptography is capable of creating a public-key cryptosystem based on lattices. Lastly, the security of multivariate-quadratic-equation-based cryptography depends on the difficulty of solving a system of multivariate polynomials over a finite field. Such cryptographic schemes use large field sizes to provide the needed security levels.

Luov is a multivariate public key cryptosystem and an adaptation of the unbalanced oil and vinegar (UOV) signature scheme, but there is a restriction on the coefficients of the public key. Instead, the scheme uses two finite fields: one is the binary field of two elements, whereas the other is its extension of degree m . F_2 is the binary field and F_{2^m} is its extension of degree m . The central map $F: F_n \times F_{2^m} \rightarrow F_o \times F_{2^m}$ is a quadratic map, where o and v satisfy $n = o + v$, $\alpha_{i,j,k}$, $\beta_{i,k}$ and γ_k are chosen from the base field F_2 , and whose components f_1, \dots, f_o are in the form $f_k(x) = \sum_{i=1}^n \sum_{j=i}^n \alpha_{i,j,k} x_i x_j + \sum_{i=1}^n \beta_{i,k} x_i + \gamma_k$.

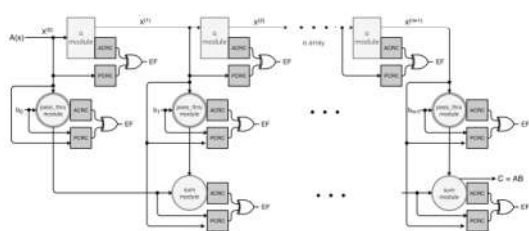


Figure-1: Finite-field multiplier with the proposed error-detection schemes based on CRC

These finite-field multiplications are very complex and require large-area footprint. Therefore, it is a complex task to implement such architectures resilient to natural and malicious faults. The aim of

this work is to provide countermeasures against natural faults and fault injections for the finite-field multipliers used in cryptosystems such as the Luov algorithm as a case study, noting that the proposed error-detection schemes can be adapted to other applications and cryptographic algorithms whose building blocks need finite-field multiplications. Readers who are interested in knowing more details about the Luov’s cryptographic algorithm are encouraged to refer to [12].

a) Proposed fault-detection architectures

The multiplication of any two elements A and B of $G F(2^m)$, following the approach in [16], can be presented as $A \cdot B \text{ mod } f(x) = \sum_{i=0}^{m-1} b_i \cdot (\sum_{\alpha} \alpha_i)$ $\text{mod } f(x) = \sum_{i=0}^{m-1} b_i \cdot X(i)$, where the set of α ’s is the polynomial basis of element A , the set of b_i ’s is the B coefficients, $f(x)$ is the field polynomial, $X(i) = \alpha \cdot X(i-1) \text{ mod } f(x)$, and $X(0) = A$. To perform finite-field multiplication, three different modules are needed: sum, α , and pass-thru modules. The sum module adds two elements in $G F(2^m)$ using m two-input XOR gates, the α module multiplies an element of $G F(2^m)$ by α and then reduces the result modulo $f(x)$, and lastly, the pass-thru module multiplies a $G F(2^m)$ element by a $G F(2)$ element. One finite-field multiplication uses a total of $m - 1$ sum modules, $m - 1$ α modules, and m pass-thru modules to get the output. Fault injection can occur in any of these modules, and formulations for parity signatures in $G F(2^m)$ are derived in [16]. Parity signatures provide an error flag (EF) on each module. The major drawback of parity signatures is that their error coverage is approximately 50%, that is, if the number of faults is even, the approach would not be able to detect the faults. This highly predictable countermeasure can be circumvented by intelligent fault injection.

In this work, our aim is the derivation of error-detection schemes that provide a broader and higher error coverage than parity signatures and explore the application of such schemes to the

Luov algorithm. Thus, we derive and apply CRC signatures [17] to the finite-field multipliers used in Luov algorithm. This would be a step forward toward detecting natural and malicious intelligent faults, especially and as discussed in this brief, considering both primitive and standardized CRCs with different fault multiplicity coverage. CRC was first proposed in 1961 and it is based on the theory

of cyclic error-correcting codes. To implement CRC, a generator polynomial $g(x)$ is required. The message becomes as the dividend, the quotient is discarded, and the remainder produces the result. In CRC, a fixed number of check bits are appended to the data and these check bits are inspected when the output is received to detect any errors. The entire finite-field multiplier with our error-detection schemes is shown in Fig. 1, where actual CRC (ACRC) and predicted CRC (PCRC) stand for ACRC signatures and PCRC signatures, respectively. In Fig. 1, only one EF is shown for clarity; however, for CRC-5, which is the case study proposed in this brief, 5 EFs are computed on each module.

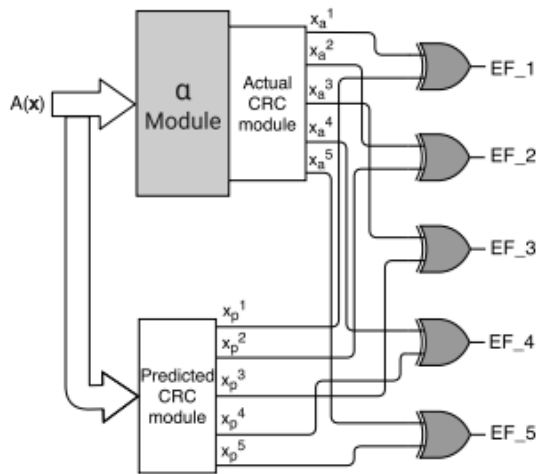


Figure-2: Proposed error-detection constructions for α module.

with its respective one to produce five EFs, which are represented as E F1–E F5. As an example, to obtain E F1, $x_1 p$ (or $a_{15} + a_{13} + a_{12} + a_{10} + a_9 + a_8 + a_6 + a_4$ for $g_0(x)$) is XORed with $x_1 a$ (or $\gamma_{14} + \gamma_{13} + \gamma_{11} + \gamma_{10} + \gamma_9 + \gamma_7 + \gamma_5 + \gamma_0$ for $g_0(x)$), which are calculated in (4) and (6), respectively. For our case study, the outputs are divided into five groups since we use CRC-5; however, if any other CRC-n is used, there will be n EFs and the actual and predicted outputs will be divided into n groups. In Table I, the CRC signatures for the different primitive polynomials are shown. We note that the choice of the utilized CRC can be tailored based on the reliability requirements and the overhead to be tolerated. In other words, for applications such as game consoles in which performance is critical (and power consumption is not because these are plugged in), one can increase the size of CRC. However, for deeply embedded systems such as

implantable and wearable medical devices, smaller CRC is preferred.

V. RESULTS

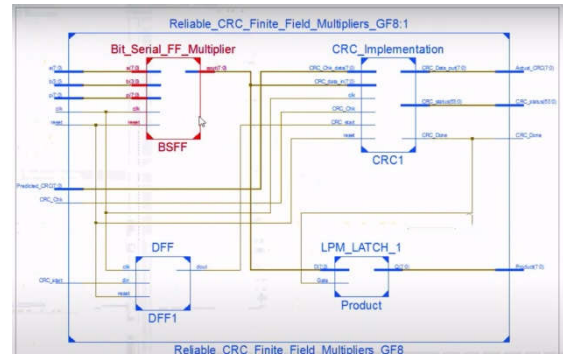


Figure-3: Proposed System

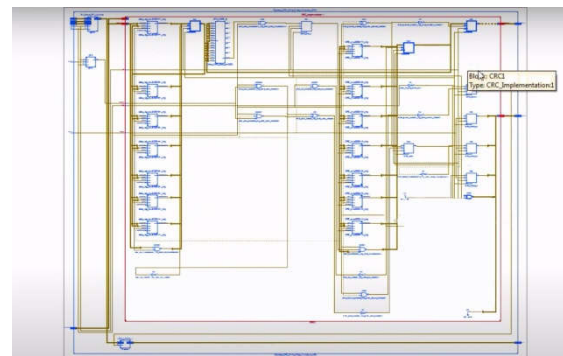


Figure-4: Schematic

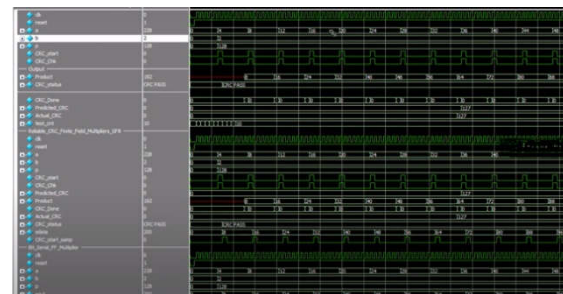


Figure-5: Output Wave forms

Table-1: Device Utilization Summary

Device Utilization Summary		Available	Utilization	Ratio (%)
Logic Elements				
Number of Logic Elements	204	207,500		1%
Number of 4-input LUTs	204	207,500		1%
Number of 6-input LUTs	0	207,500		0%
Number of 8-input LUTs	0	207,500		0%
Number of 10-input LUTs	0	207,500		0%
Number of 12-input LUTs	0	207,500		0%
Number of 14-input LUTs	0	207,500		0%
Number of 16-input LUTs	0	207,500		0%
Number of 18-input LUTs	0	207,500		0%
Number of 20-input LUTs	0	207,500		0%
Number of 22-input LUTs	0	207,500		0%
Number of 24-input LUTs	0	207,500		0%
Number of 26-input LUTs	0	207,500		0%
Number of 28-input LUTs	0	207,500		0%
Number of 30-input LUTs	0	207,500		0%
Number of 32-input LUTs	0	207,500		0%
Number of 34-input LUTs	0	207,500		0%
Number of 36-input LUTs	0	207,500		0%
Number of 38-input LUTs	0	207,500		0%
Number of 40-input LUTs	0	207,500		0%
Number of 42-input LUTs	0	207,500		0%
Number of 44-input LUTs	0	207,500		0%
Number of 46-input LUTs	0	207,500		0%
Number of 48-input LUTs	0	207,500		0%
Number of 50-input LUTs	0	207,500		0%
Number of 52-input LUTs	0	207,500		0%
Number of 54-input LUTs	0	207,500		0%
Number of 56-input LUTs	0	207,500		0%
Number of 58-input LUTs	0	207,500		0%
Number of 60-input LUTs	0	207,500		0%
Number of 62-input LUTs	0	207,500		0%
Number of 64-input LUTs	0	207,500		0%
Number of 66-input LUTs	0	207,500		0%
Number of 68-input LUTs	0	207,500		0%
Number of 70-input LUTs	0	207,500		0%
Number of 72-input LUTs	0	207,500		0%
Number of 74-input LUTs	0	207,500		0%
Number of 76-input LUTs	0	207,500		0%
Number of 78-input LUTs	0	207,500		0%
Number of 80-input LUTs	0	207,500		0%
Number of 82-input LUTs	0	207,500		0%
Number of 84-input LUTs	0	207,500		0%
Number of 86-input LUTs	0	207,500		0%
Number of 88-input LUTs	0	207,500		0%
Number of 90-input LUTs	0	207,500		0%
Number of 92-input LUTs	0	207,500		0%
Number of 94-input LUTs	0	207,500		0%
Number of 96-input LUTs	0	207,500		0%
Number of 98-input LUTs	0	207,500		0%
Number of 100-input LUTs	0	207,500		0%
Number of 102-input LUTs	0	207,500		0%
Number of 104-input LUTs	0	207,500		0%
Number of 106-input LUTs	0	207,500		0%
Number of 108-input LUTs	0	207,500		0%
Number of 110-input LUTs	0	207,500		0%
Number of 112-input LUTs	0	207,500		0%
Number of 114-input LUTs	0	207,500		0%
Number of 116-input LUTs	0	207,500		0%
Number of 118-input LUTs	0	207,500		0%
Number of 120-input LUTs	0	207,500		0%
Number of 122-input LUTs	0	207,500		0%
Number of 124-input LUTs	0	207,500		0%
Number of 126-input LUTs	0	207,500		0%
Number of 128-input LUTs	0	207,500		0%
Number of 130-input LUTs	0	207,500		0%
Number of 132-input LUTs	0	207,500		0%
Number of 134-input LUTs	0	207,500		0%
Number of 136-input LUTs	0	207,500		0%
Number of 138-input LUTs	0	207,500		0%
Number of 140-input LUTs	0	207,500		0%
Number of 142-input LUTs	0	207,500		0%
Number of 144-input LUTs	0	207,500		0%
Number of 146-input LUTs	0	207,500		0%
Number of 148-input LUTs	0	207,500		0%
Number of 150-input LUTs	0	207,500		0%
Number of 152-input LUTs	0	207,500		0%
Number of 154-input LUTs	0	207,500		0%
Number of 156-input LUTs	0	207,500		0%
Number of 158-input LUTs	0	207,500		0%
Number of 160-input LUTs	0	207,500		0%
Number of 162-input LUTs	0	207,500		0%
Number of 164-input LUTs	0	207,500		0%
Number of 166-input LUTs	0	207,500		0%
Number of 168-input LUTs	0	207,500		0%
Number of 170-input LUTs	0	207,500		0%
Number of 172-input LUTs	0	207,500		0%
Number of 174-input LUTs	0	207,500		0%
Number of 176-input LUTs	0	207,500		0%
Number of 178-input LUTs	0	207,500		0%
Number of 180-input LUTs	0	207,500		0%
Number of 182-input LUTs	0	207,500		0%
Number of 184-input LUTs	0	207,500		0%
Number of 186-input LUTs	0	207,500		0%
Number of 188-input LUTs	0	207,500		0%
Number of 190-input LUTs	0	207,500		0%
Number of 192-input LUTs	0	207,500		0%
Number of 194-input LUTs	0	207,500		0%
Number of 196-input LUTs	0	207,500		0%
Number of 198-input LUTs	0	207,500		0%
Number of 200-input LUTs	0	207,500		0%
Number of 202-input LUTs	0	207,500		0%
Number of 204-input LUTs	0	207,500		0%
Number of 206-input LUTs	0	207,500		0%
Number of 208-input LUTs	0	207,500		0%
Number of 210-input LUTs	0	207,500		0%
Number of 212-input LUTs	0	207,500		0%
Number of 214-input LUTs	0	207,500		0%
Number of 216-input LUTs	0	207,500		0%
Number of 218-input LUTs	0	207,500		0%
Number of 220-input LUTs	0	207,500		0%
Number of 222-input LUTs	0	207,500		0%
Number of 224-input LUTs	0	207,500		0%
Number of 226-input LUTs	0	207,500		0%
Number of 228-input LUTs	0	207,500		0%
Number of 230-input LUTs	0	207,500		0%
Number of 232-input LUTs	0	207,500		0%
Number of 234-input LUTs	0	207,500		0%
Number of 236-input LUTs	0	207,500		0%
Number of 238-input LUTs	0	207,500		0%
Number of 240-input LUTs	0	207,500		0%
Number of 242-input LUTs	0	207,500		0%
Number of 244-input LUTs	0	207,500		0%
Number of 246-input LUTs	0	207,500		0%
Number of 248-input LUTs	0	207,500		0%
Number of 250-input LUTs	0	207,500		0%
Number of 252-input LUTs	0	207,500		0%
Number of 254-input LUTs	0	207,500		0%
Number of 256-input LUTs	0	207,500		0%
Number of 258-input LUTs	0	207,500		0%
Number of 260-input LUTs	0	207,500		0%
Number of 262-input LUTs	0	207,500		0%
Number of 264-input LUTs	0	207,500		0%
Number of 266-input LUTs	0	207,500		0%
Number of 268-input LUTs	0	207,500		0%
Number of 270-input LUTs	0	207,500		0%
Number of 272-input LUTs	0	207,500		0%
Number of 274-input LUTs	0	207,500		0%
Number of 276-input LUTs	0	207,500		0%
Number of 278-input LUTs	0	207,500		0%
Number of 280-input LUTs	0	207,500		0%
Number of 282-input LUTs	0	207,500		0%
Number of 284-input LUTs	0	207,500		0%
Number of 286-input LUTs	0	207,500		0%
Number of 288-input LUTs	0	207,500		0%
Number of 290-input LUTs	0	207,500		0%
Number of 292-input LUTs	0	207,500		0%
Number of 294-input LUTs	0	207,500		0%
Number of 296-input LUTs	0	207,500		0%
Number of 298-input LUTs	0	207,500		0%
Number of 300-input LUTs	0	207,500		0%
Number of 302-input LUTs	0	207,500		0%
Number of 304-input LUTs	0	207,500		0%
Number of 306-input LUTs	0	207,500		0%
Number of 308-input LUTs	0	207,500		0%
Number of 310-input LUTs	0	207,500		0%
Number of 312-input LUTs	0	207,500		0%
Number of 314-input LUTs	0	207,500		0%
Number of 316-input LUTs	0	207,500		0%
Number of 318-input LUTs	0	207,500		0%
Number of 320-input LUTs	0	207,500		0%
Number of 322-input LUTs	0	207,500		0%
Number of 324-input LUTs	0	207,500		0%
Number of 326-input LUTs	0	207,500		0%
Number of 328-input LUTs	0	207,500		0%
Number of 330-input LUTs	0	207,500		0%
Number of 332-input LUTs	0	207,500		0%
Number of 334-input LUTs	0	207,500		0%
Number of 336-input LUTs	0	207,500		0%
Number of 338-input LUTs	0	207,500		0%
Number of 340-input LUTs	0	207,500		0%
Number of 342-input LUTs	0	207,500		0%
Number of 344-input LUTs	0	207,500		0%
Number of 346-input LUTs	0	207,500		0%
Number of 348-input LUTs	0	207,500		0%
Number of 350-input LUTs	0	207,500		0%
Number of 352-input LUTs	0	207,500		0%
Number of 354-input LUTs	0	207,500		0%
Number of 356-input LUTs	0	207,500		0%
Number of 358-input LUTs	0	207,500		0%
Number of 360-input LUTs	0	207,500		0%
Number of 362-input LUTs	0	207,500		0%
Number of 364-input LUTs	0	207,500		0%
Number of 366-input LUTs	0	207,500		0%
Number of 368-input LUTs	0	207,500		0%
Number of 370-input LUTs	0	207,500		0%
Number of 372-input LUTs	0	207,500		0%
Number of 374-input LUTs	0	207,500		0%
Number of 376-input LUTs	0	207,500		0%
Number of 378-input LUTs	0	207,500		0%
Number of 380-input LUTs	0	207,500		0%
Number of 382-input LUTs	0	207,500		0%
Number of 384-input LUTs	0	207,500		0%
Number of 386-input LUTs	0	207,500		0%
Number of 388-input LUTs	0	207,500		0%
Number of 390-input LUTs	0	207,500		0%
Number of 392-input LUTs	0	207,500		0%
Number of 394-input LUTs	0	207,500		0%
Number of 396-input LUTs	0	207,500		0%
Number of				

Table-2: Comparison of CRC – Based Error Constructions for Finite Field Multipliers

	Comparisons of Reliable CRC-Based Error Detection Constructions for Finite Field Multipliers	
	GF8 - CRC	GF32 CRC
Number of Slice Registers	56	214
Number of Slice LUTs	140	616
Number of Occupied Slices	43	229
IOBs	113	245
Delay (ns)	3.102	3.665
Power (W)	3.296	3.300

VI. CONCLUSION

In this work, we have derived error-detection schemes for the finite-field multipliers used in post quantum cryptographic algorithms such as Luov, noting that the proposed error-detection schemes can be adapted to other applications and cryptographic algorithms whose building blocks need finite-field multiplications. The error-detection architectures proposed in this work are based on CRC-5 signatures and we have performed software implementations for the sake of verification. Additionally, we have explored and studied both primitive and standardized generator polynomials for CRC-5, comparing the complexity for each of them. We have embedded the proposed error-detection schemes into the original finite-field multipliers of the Luov's algorithm, obtaining high error coverage with acceptable overhead.

REFERENCES

- [1] J. L. Danger et al., "On the performance and security of multiplication in $GF(2^N)$," *Cryptography*, vol. 2, no. 3, pp. 25–46, 2018.
- [2] M. Mozaffari-Kermani and A. Reyhani-Masoleh, "Reliable hardware architectures for the third-round SHA-3 finalist Grostl benchmarked on FPGA platform," in *Proc. DFT*, Oct. 2011, pp. 325–331.
- [3] M. Mozaffari-Kermani and A. Reyhani-Masoleh, "A low-cost S-box for the advanced encryption standard using normal basis," in *Proc. IEEE Int. Conf. Electro/Inf. Technol.*, Jun. 2009, pp. 52–55.
- [4] M. Yasin, B. Mazumdar, S. S. Ali, and O. Sinanoglu, "Security analysis of logic encryption against the most effective side-channel attack: DPA," in *Proc. IEEE Int. Symp. Defect Fault*

Tolerance VLSI Nanotechnol. Syst. (DFTS), Oct. 2015, pp. 97–102.

- [5] M. Mozaffari-Kermani, R. Azarderakhsh, A. Sarker, and A. Jalali, "Efficient and reliable error detection architectures of hash-counter-hash tweakable enciphering schemes," *ACM Trans. Embedded Comput. Syst.*, vol. 17, no. 2, pp. 54:1–54:19, May 2018.
- [6] M. Mozaffari-Kermani, R. Azarderakhsh, and A. Aghaie, "Reliable and error detection architectures of Pomaranch for false-alarm-sensitive cryptographic applications," *IEEE Trans. Very Large Scale Integr. (VLSI) Syst.*, vol. 23, no. 12, pp. 2804–2812, Dec. 2015.
- [7] A. Sarker, M. Mozaffari-Kermani, and R. Azarderakhsh, "Hardware constructions for error detection of number-theoretic transform utilized in secure cryptographic architectures," *IEEE Trans. Very Large Scale Integr. (VLSI) Syst.*, vol. 27, no. 3, pp. 738–741, Mar. 2019.
- [8] M. Mozaffari-Kermani, R. Azarderakhsh, and A. Aghaie, "Fault detection architectures for post-quantum cryptographic stateless hash-based secure signatures benchmarked on ASIC," *ACM Trans. Embedded Comput. Syst.*, vol. 16, no. 2, pp. 59:1–59:19, Dec. 2016.
- [9] M. Mozaffari-Kermani and R. Azarderakhsh, "Reliable hash trees for post-quantum stateless cryptographic hash-based signatures," in *Proc. IEEE Int. Symp. Defect Fault Tolerance VLSI Nanotechnol. Syst. (DFTS)*, Oct. 2015, pp. 103–108.
- [10] M. M. Kermani and R. Azarderakhsh, "Reliable architecture-oblivious error detection schemes for secure cryptographic GCM structures," *IEEE Trans. Rel.*, vol. 68, no. 4, pp. 1347–1355, Dec. 2019.
- [11] A. A. Kamal and A. M. Youssef, "Strengthening hardware implementations of NTRUEncrypt against fault analysis attacks," *J. Cryptograph. Eng.*, vol. 3, no. 4, pp. 227–240, Nov. 2013.
- [12] A. Kipnis, J. Patarin, and L. Goubin, "Unbalanced oil and vinegar signature schemes," in

Proc. Int. Conf. Theory Appl. Cryptograph. Techn. Berlin, Germany: Springer, 1999, pp. 206–222.

[13] D. Moody, “Post-quantum cryptography: NIST’s plan for the future,” Tech. Rep., Feb. 2016. [Online]. Available: <https://csrc.nist.gov/csrc/media/projects/post-quantum-cryptography/documents/pqcrypto-2016-presentation.pdf>

[14] D. Moody, “Post-quantum cryptography: Round 2 submissions,” Tech. Rep., Mar. 2019. [Online]. Available: <https://csrc.nist.gov/CSRC/media/Presentations/Round-2-of-the-NIST-PQC-Competition-Whatwas-NIST/images-media/pqcrypto-may2019-moody.pdf>

[15] D. J. Bernstein, “Post-quantum cryptography,” in *Encyclopedia of Cryptography and Security*, H. C. A. van Tilborg and S. Jajodia, Eds. Boston, MA, USA: Springer, 2011, pp. 949–950, doi: 10.1007/978-1-4419-5906-5_386.

[16] A. Reyhani-Masoleh and M. A. Hasan, “Error detection in polynomial basis multipliers over binary extension fields,” in *Proc. CHES*, 2002, pp. 515–528.

[17] EPC Radio-Frequency Identity Protocols Class-1 Generation-2 UHF RFID Protocol for Communications at 860 MHz 960 MHz, EPC Global, Brussels, Belgium, Version 1.0.23, 2008.

[18] T. V. Ramabadran and S. S. Gaitonde, “A tutorial on CRC computations,” *IEEE Micro*, vol. 8, no. 4, pp. 62–75, Aug. 1988.

[19] S. Subramanian, M. Mozaffari-Kermani, R. Azarderakhsh, and M. Nojoumian, “Reliable hardware architectures for cryptographic block ciphers LED and HIGHT,” *IEEE Trans. Comput.-Aided Design Integr. Circuits Syst.*, vol. 36, no. 10, pp. 1750–1758, Oct. 2017.